Scientific Research Publishing

Journal of Computer and Communications, 2025, 13(6), 234-250
https://www.scirp.org/journal/jcc
ISSN Online: 2327-5227
ISSN Print: 2327-5219

Simulation Study of GNSS-R-Based Marine Oil Spill Detection Considering Sea Surface Asymmetry

Jintao Yu, Bin Wang, Dongmei Song

College of Oceanography and Space Informatics, China University of Petroleum (East China), Qingdao, China
Email: b23160004@s.upc.edu.cn, wangbin007@upc.edu.cn, songdongmei@upc.edu.cn

How to cite this paper: Yu, J.T., Wang, B. and Song, D.M. (2025) Simulation Study of GNSS-R-Based Marine Oil Spill Detection Considering Sea Surface Asymmetry. *Journal of Computer and Communications*, **13**, 234-250.
https://doi.org/10.4236/jcc.2025.136016

Received: May 18, 2025
Accepted: June 27, 2025
Published: June 30, 2025

Abstract

Marine oil spills cause severe ocean pollution. When oil spreads over the sea surface, it hinders optical processes within the ocean and consumes large amounts of dissolved oxygen during decomposition, leading to massive marine life mortality. To mitigate the impact of oil spill disasters, real-time and accurate monitoring is of great significance for protecting the marine ecosystem. Traditional optical and radar remote sensing techniques often suffer from long revisit times, making it difficult to respond swiftly to offshore oil spill incidents, thus exacerbating marine pollution. In contrast, Global Navigation Satellite System Reflectometry (GNSS-R) offers all-weather, real-time monitoring capabilities, making it more suitable for detecting oil spills on the sea surface. This study focuses on the oil spill incident caused by the Symphony cargo ship on April 27, 2021. Considering the asymmetry of the actual sea surface, the bistatic scattering coefficient of the oil-covered sea surface is calculated using the KA-GO model. Combined with the Z-V scattering model and a sea surface/oil slick Mean Square Slope (MSS) model, a Delay-Doppler Map (DDM) reflecting oil spill features is generated. Simulation results demonstrate that DDMs can effectively detect oil spill areas, validating the feasibility of GNSS-R for this application. Furthermore, the study reveals that sea surface wind speed significantly influences simulation results: when wind speed exceeds 2 m/s, the differences in MSS and scattering coefficients between oil-covered and clean sea surfaces become more pronounced, decreasing with higher wind speeds. Finally, CYGNSS (Cyclone GNSS) satellite data is used to verify the consistency of oil spill-induced GNSS-R signal patterns derived from simulation, providing both theoretical and methodological references for applying GNSS-R in marine oil spill monitoring.

Keywords

GNSS-R, Marine Oil Spill, Wind Speed, Delay-Doppler Map

1. Introduction

Frequent marine oil spill incidents pose a serious threat to both marine ecosystems and coastal human societies. Oil spills not only pollute seawater, leading to the death of marine organisms and the destruction of habitats, but also cause significant economic losses to industries such as fisheries and tourism [1] [2]. Therefore, effectively monitoring and responding quickly to marine oil spills has become an urgent issue in mitigating their environmental and economic impacts.

Traditional marine oil spill monitoring methods mainly rely on optical and microwave remote sensing technologies. Optical remote sensing can provide high-resolution imagery under clear weather conditions; however, its performance is severely limited under cloudy conditions due to its susceptibility to weather. Although microwave remote sensing (such as Synthetic Aperture Radar, SAR) enables all-weather monitoring [3] [4], its use is often restricted by high system complexity and cost, limiting its application in large-scale and real-time monitoring. Thus, there is an urgent need for an efficient, low-cost, and all-weather monitoring technique to complement existing methods. The Global Navigation Satellite System Reflectometry (GNSS-R) has garnered increasing attention in recent years for ocean remote sensing, owing to its advantages such as abundant signal sources, wide coverage, low cost, and immunity to weather conditions [5] [6]. GNSS-R utilizes the microwave signals emitted by navigation satellites, which reflect off the ocean surface and are captured by receiving equipment. By analyzing the characteristics of the reflected signals, it is possible to monitor the state of the sea surface. Compared with traditional remote sensing technologies, GNSS-R exhibits strong anti-interference capabilities and supports large-scale, real-time ocean monitoring, as its signal sources are derived from multiple navigation satellites.

Since 1993, when scholars such as Manuel Martin Neira [7] first proposed the idea of using GPS scattering signals to measure sea surface height, GNSS-R remote sensing technology has developed into an emerging research field. During the past 20 years, through various observation platforms, such as shore-based, airborne, and satellite-based, this technology has made important breakthroughs in signal reception, parameter inversion, and surface imaging, and has been successfully applied to many fields, such as sea surface wind field [8]-[11], sea ice monitoring [12]-[14], and soil moisture [15]-[17]. In recent years, research on GNSS-R technology in marine oil spill monitoring has gradually been carried out. Scholars at home and abroad have carried out a series of studies on the application of GNSS-R technology to marine oil spill monitoring. Valencia *et al.* [18] [19] modelled the oil spill sea surface, simulated the DDM and used the inverse convolution to obtain the distribution of scattering coefficients of the sea surface for the detection

of oil spill. On this basis, Chen Li *et al.* [20] corrected the sea surface scattering coefficient distribution obtained by DDM inverse convolution to improve the scattering coefficient extraction accuracy. Li and Huang *et al.* [21] applied the spatial integration approach (SIA) in the technique of simulation and detection of oil spills on the sea surface using GNSS-R information. Chen Shanshan *et al.* [22] conducted a shore-based simulation study of GNSS-R sea surface oil spill detection using remote sensing images of the 2013 Qingdao, China, marine oil spill accident as the detection target of the simulation experiment. The study combined the Z-V scattering model and the mean-square slope model of seawater/oil spill to establish the time-delay-Doppler map that can reflect the characteristics of the GNSS scattering signals of the sea surface condition, and verified the feasibility of the use of the GNSS reflection signals for the detection of oil spill on the sea surface. China's Beidou signal is also an important GNSS-R signal source, Zhang Yun *et al.* [23] assessed the feasibility of Beidou Navigation Satellite System reflected signals to detect oil slicks, and carried out a coastal simulation experimental study on the distribution of oil slicks from an oil pipeline explosion accident. Jia Ziying *et al.* [24] established a model for oil spill detection at sea in three-antenna observation mode from a shore-based perspective, combining the partial depolarization phenomenon of electromagnetic waves and the mapping relationship between reflectivity and sea surface roughness eigenfunctions, to determine the presence of an oil spill based on the relative permittivity of the inverse-performance target waters. Sun Qiming *et al.* [25], in order to study the detection method of shore-based oil spill area, inverted the relative permittivity of the sea surface within the flashing area by establishing the mapping relationship between the correlation power, reflectivity and the three characteristic parameters of the sea surface, and carried out the oil spill detection work in this way.

At present, domestic research on GNSS-R-based marine oil spill detection is still in its early stages, and experimental data on GNSS-R observations of oil spills remain scarce. To validate the potential of GNSS-R technology in marine oil spill monitoring, this study simulates a satellite-based GNSS-R oil spill detection process using the 2021 Symphony cargo vessel oil spill as a case study. The simulation is based on two-dimensional correlation power in the Delay-Doppler domain to evaluate the detectability of oil spills on the ocean surface using GNSS-R technology.

2. GNSS-R Oil Spill Simulation Principles

2.1. Scattering Signal Measurement Geometry

The GNSS reflected signal monitoring system consists of three components: navigation satellites, receiving antennas, and the reflecting surface. Due to the high orbital altitude of GNSS satellites, the transmitted signals can be approximated as plane waves when they reach the Earth's surface. On an ideal, infinitely large Earth surface, these signals undergo specular reflection, with the GNSS reflected signal dominated by the specular component. The signal received by the antenna is formed by the combined scattering contributions from various reflection elements

on the sea surface. Each reflection element corresponds to a unique delay and Doppler shift relative to the specular reflection point. Thus, the observed surface is divided along two dimensions: iso-delay lines and iso-Doppler lines. In the presence of an oil spill on the sea surface, these signal components are altered. By applying Delay-Doppler Map (DDM) techniques, these variations can be accurately measured and extracted, enabling the inversion and detection of the spatial distribution of the oil spill.

2.2. DDM Principle for Oil Spill Detection

According to the GNSS ocean surface scattering Z-V model based on the Kirchhoff approximation theory, the scattered sea surface signals are composed of components with different time delays and Doppler shifts. When an oil spill is present, these signal components change, and this variation can be characterized by the correlation power of the scattered signal at different code delays and Doppler frequencies.

In 2000, Zavortny and Voronovich developed a two-dimensional delay-Doppler correlation power model for GNSS ocean surface scattering signals based on the bistatic radar equation and the Kirchhoff approximation using a geometric optics approach [26]. This Z-V model is now widely applied in various GNSS-R ocean remote sensing applications, such as sea surface wind speed retrieval, sea ice monitoring, and oil spill detection. The model is expressed as follows:

$$\left\langle \left| Y(\Delta\tau,\Delta f) \right|^2 \right\rangle = T_i^2 \iint_Z \frac{\left| S(\Delta f) \right|^2 \sigma^0(r) \Lambda^2(\Delta\tau) D^2(r)}{4\pi R_R^2(r) R_T^2(r)} d_r^2 \tag{1}$$

where T_i the coherent integration time, $D(r)$ is the antenna gain of the receiver, Λ is the autocorrelation function, S is the Doppler filtering function, $R_T(r)$ and $R_R(r)$ are the distances of the GNSS satellites and receiver to the scattering points, respectively, Δf and $\Delta\tau$ represent the Doppler shifts and time delays of the scattering points on the reflecting surface with respect to the specular reflection points, respectively. Doppler shift and time delay, r is the position vector of the scattering point. The specific equations are expanded as follows.

(1) MSS Model:

According to the MSS (Mean Square Slope) model proposed by Cox & Munk, the presence of oil on the sea surface significantly affects the MSS [27]. For clean seawater, the MSS is a function of the 10-meter wind speed, expressed as:

$$\begin{aligned} \sigma_{c,c}^2 &= 0.003 + 1.92 \cdot 10^{-3} U_{10} \\ \sigma_{u,c}^2 &= 3.16 \cdot 10^{-3} U_{10} \end{aligned} \tag{2}$$

When oil is present on the sea surface, it alters the surface roughness and consequently changes the MSS. For oil-covered seas, the relationship becomes:

$$\begin{aligned} \sigma_{c,s}^2 &= 0.003 + 0.84 \cdot 10^{-3} U_{10} \\ \sigma_{u,s}^2 &= 0.005 + 0.78 \cdot 10^{-3} U_{10} \end{aligned} \tag{3}$$

where: the first subscript u of the MSS denotes upwind and c denotes cross-

wind; the second subscript s, c of the MSS denotes oil spill and seawater on the sea surface, respectively; and U_{10} is the wind speed at a sea surface height of 10 m.

(2) PDF Model

The ECXI (Earth-Centered, X-Z Incidence) coordinate system is used in the study, and assuming that the wind direction is along the X-axis, the expression of the probability distribution function of the sea surface gradient for each scattering point is given by

$$P_{pdf}(-\frac{q_\perp}{q_z}) = \frac{1}{2\pi\sqrt{\sigma_u^2\sigma_c^2}} \cdot \exp\left[-\frac{1}{2}\left[\frac{(-q_{\perp,c}/q_z)^2}{\sigma_c^2} + \frac{(-q_{\perp,u}/q_z)^2}{\sigma_u^2}\right]\right] \tag{4}$$

where σ_c^2 and σ_u^2 represent the MSS in the up-wind and cross-wind directions, respectively (based on the ECXI system).

(3) Scattering coefficient σ⁰

σ⁰ refers to the scattering coefficient corresponding to each scattering point within the observation area.

$$\sigma^0(r) = \pi|\Re|^2\left(\frac{|q|}{q_z}\right)^4 P_{pdf}\left(-\frac{q_\perp}{q_z}\right) \tag{5}$$

where q is the scattering vector of the transmitter and receiver at a fixed position on the reflecting surface, which can also be considered as a function of the plane coordinate $\vec{\rho}$, $\Re$ is the Fresnel reflection coefficient, $q_\perp$ is the horizontal component of the scattering vector, q_z is the z-direction component of the scattering vector, and $P_{pdf}(-q_\perp/q_z)$ is the probability density function of the sea surface slope.

(4) Σ function

Before the receiver receives the scattering signal, where the expression for the energy of each scattering point is as follows.

$$\Sigma(\Delta\tau, \Delta f) = \frac{T_i^2 D^2(r)\sigma^0(r)}{4\pi R_R^2(r) R_T^2(r)} ds \tag{6}$$

where T_i is the coherent integration time, $D(r)$ is the antenna gain of the receiver, and r is the position vector of the scattering point.

(5) Convolution of Σ and x functions

Using the Z-V model based on Kirchhoff's approximate geometrical optics theory, the time-delay-Doppler two-dimensional correlation power model of the GNSS sea surface scattered signal is constructed as follows

$$\left\langle \left|Y(\Delta\tau, \Delta f)\right|^2 \right\rangle = \Sigma(\Delta\tau, \Delta f) * \chi^2(\Delta\tau, \Delta f) \tag{7}$$

$$\chi^2(\Delta\tau, \Delta f) = \Lambda^2(\Delta\tau) \cdot \left|S(\Delta f)\right|^2 \tag{8}$$

where $*$ denotes the 2D convolution, χ is the blurring function.

According to the above equation, under specific wind speed and wind direction conditions, the presence of an oil spill on the sea surface alters the local mean square

slope (MSS), resulting in significant differences compared to clean seawater. This change in MSS further affects the surface roughness characteristics of each scattering point within the observation area, thereby leading to variations in the corresponding coefficient. The modified scattering coefficient field can then be used as input to the Z-V model, enabling a more accurate representation of scattering characteristics under different sea surface conditions. This, in turn, supports the simulation of the Delay-Doppler Map (DDM) and provides a physical basis for sea surface state identification and oil spill detection.

3. Experimental Design

3.1. Simulation Experimental Scenario

This study takes the oil spill incident caused by the "Symphony" cargo ship on April 27, 2021, near the coast of Qingdao, China, as the research subject, using it as a representative application scenario for GNSS-R-based sea surface oil spill monitoring. Remote sensing data of the oil spill is used as model input, and the main distribution area of the spill is extracted from Sentinel-1 satellite radar imagery, as shown in **Figure 1**.

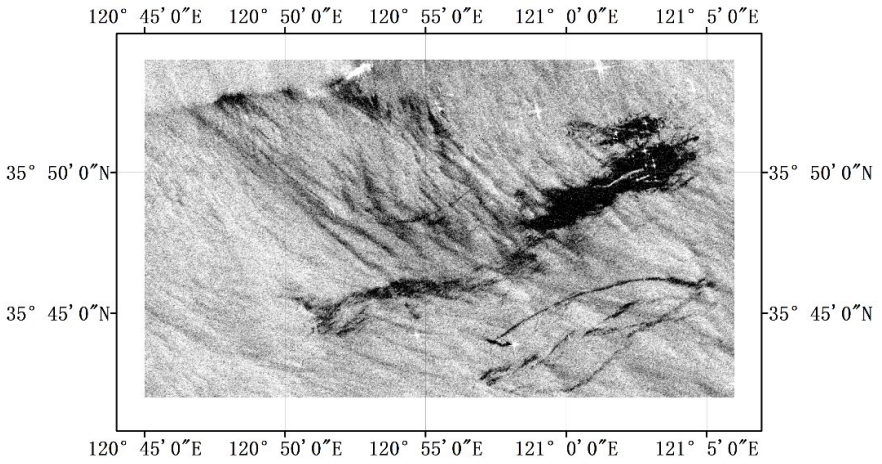

Figure 1. Distribution of oil spill areas on the sea surface.

The specific simulation experimental parameters for this experiment are shown in **Table 1**.

Table 1. Main parameters of the simulation experiment.

Parameter name	Specific value	Unit
GPS satellite coordinates	(−6,985,915, 18,179,300, 17,885,949)	m
Receiver coordinates	(−2,988,392, 4,796,629, 3,945,131)	m
GPS satellite velocity	(−1009, −2074, 1735)	m/s
Receiver velocity	(−6158, −3721, −111)	m/s
Delay resolution	1	chips

Continued

Doppler resolution	500	Hz
Antenna gain scaling factor	1	\
Scattering area range	[−25, 25]	km
Scattering unit resolution	1	km
Integration time	1	ms

3.2. GNSS-R Oil Spill Simulation Technical Workflow

This study conducts a simulation of GNSS-R technology applied to marine oil spill monitoring, using a real oil spill event as the research background. First, wind speed and direction data over the study area are input, and the Cox & Munk model is employed to calculate the mean square slope (MSS) of both clean seawater and oil-covered surfaces, thereby characterizing the roughness under different sea conditions. A probability density function (PDF) model is then used to describe the statistical distribution of sea surface slopes in each region, from which the corresponding sea surface scattering coefficients (σ^0) are derived. During the scattering coefficient calculation, the directional asymmetry of the sea surface caused by wind is further considered. Based on the actual spatial distribution of wind speed in the study area, the initially estimated σ^0 values are corrected to obtain scattering coefficients that better reflect real sea surface conditions.

Subsequently, the positions and velocities of the GNSS satellite and receiver are used to accurately locate the specular reflection point and surrounding scattering points within the observation area. Combined with the corrected scattering coefficients and the scattering geometry, the reflected signal power from the sea surface is computed, and a Delay-Doppler Map (DDM) is generated accordingly. By analyzing and interpreting the power distribution patterns in the DDM, the spatial extent and characteristics of the oil spill are extracted and identified. The structural framework of the simulation process is illustrated in **Figure 2**.

4. Results and Analyses

4.1. Verification of Simulation Results

According to the sea surface oil spill distribution shown in **Figure 1** and the experimental parameters listed in **Table 1**, a detailed monitoring simulation scheme was developed. First, the mean square slope (MSS) values of the oil-contaminated area and the clean seawater area were calculated using Equation (2) and Equation (3), respectively, to characterize the differences in surface roughness under varying sea conditions. The obtained MSS values were then substituted into Equation (4) to construct the slope probability density function, which was further combined with Equation (5) to derive the scattering coefficients for each region. The final distribution of the sea surface scattering coefficients is shown in **Figure 3**.

As illustrated in **Figure 3**, the scattering coefficients in the oil spill region are significantly higher than those in the clean seawater area. This is because the

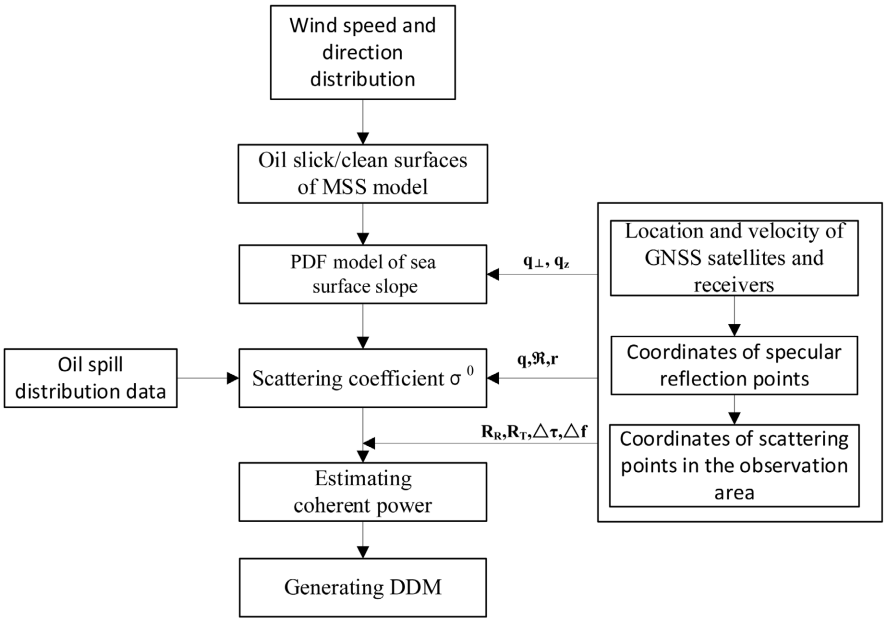

Figure 2. GNSS-R oil spill simulation flowchart.

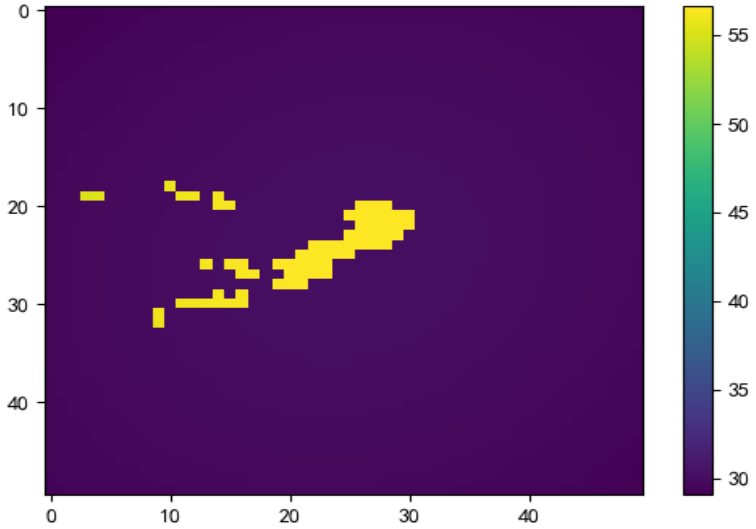

Figure 3. Distribution of oil spill areas on the sea surface.

presence of an oil film on the sea surface reduces the surface tension of seawater, effectively suppressing the generation of capillary waves and small-scale gravity waves, thereby weakening their scattering contribution to the incident electromagnetic waves. As a result, the forward scattering of GNSS signals is enhanced while the backward scattering is reduced, leading to a distinctive change in the scattering energy distribution in the Delay-Doppler Map (DDM) compared to that of a clean sea surface.

By fully considering the asymmetry of the actual sea surface, and based on the scattering coefficient distribution shown in the experimental scenario in **Figure 3**, the scattering signal Delay-Doppler Map (DDM) containing oil spill features was extracted in both the delay domain and Doppler frequency domain using the

mathematical model established by Equation (1). **Figure 4** presents the simulated DDM result, where the horizontal axis represents code delay (in chips), and the vertical axis represents Doppler frequency shift (in Hz). The color intensity indicates the power strength of the GNSS sea surface scattering signal at different positions. From **Figure 4**, the oil spill region on the sea surface can be clearly distinguished, demonstrating the feasibility and effectiveness of using GNSS-R technology for marine oil spill detection. For comparison, **Figure 5** shows the DDM image under clean sea surface conditions.

In addition, in order to elucidate the performance pattern of GNSS-R in detecting

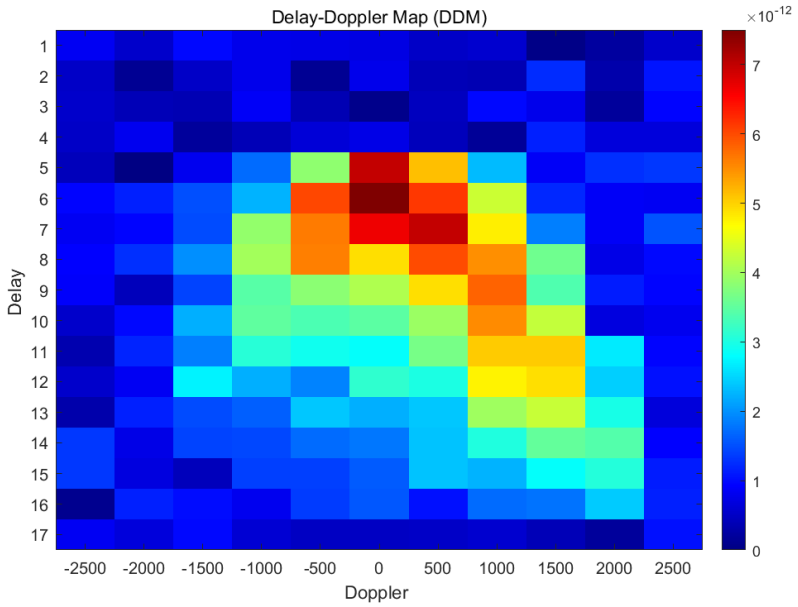

Figure 4. DDM for inversion of oil spill distributione.

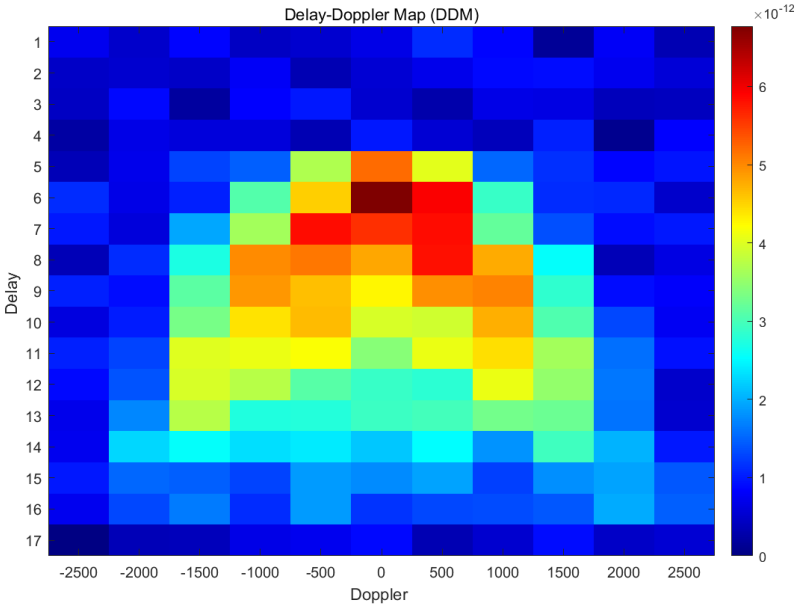

Figure 5. DDM for inversion of clean sea surface distribution.

oil spill characteristic parameters under various wind speed conditions, clean and oil-covered sea surface were simulated based on the parameters listed in **Table 1** and the SAR images shown in **Figure 1**. **Figure 6** shows the comparison of sea surface MSS for oil-covered and clean sea surface under different wind speed conditions. **Figure 6** shows the comparison of scattering coefficients for oil-covered and clean sea surface for different wind speed conditions. These comparisons are critical to understanding how oil spills change sea surface characteristics, which in turn affects the scattering characteristics detected by GNSS-R.

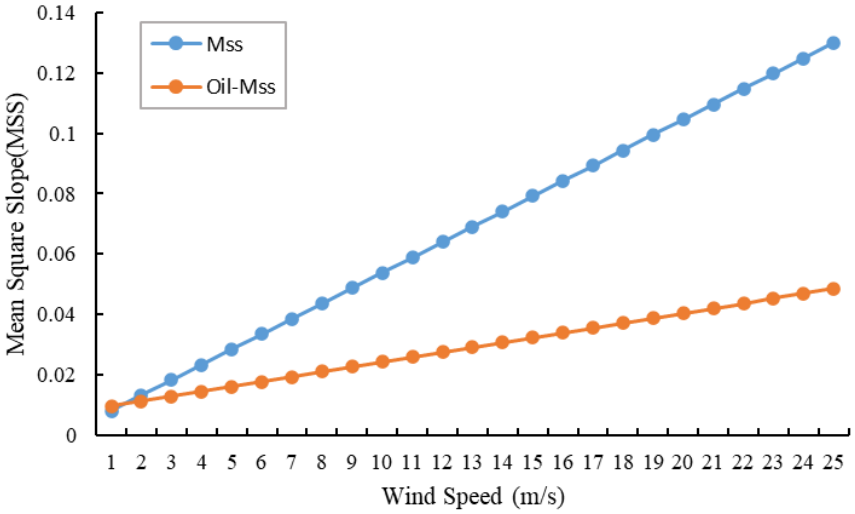

Figure 6. Comparison results of MSS between oil film covered sea surface and clean sea surface at different wind speeds.

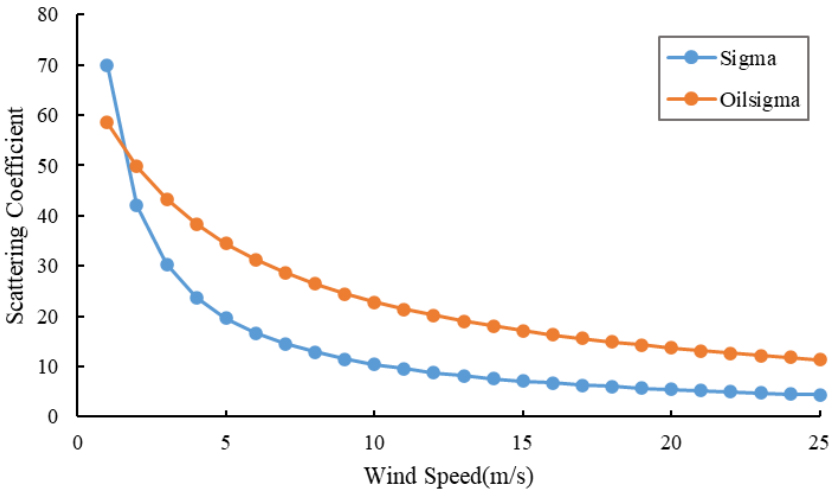

Figure 7. Comparison of scattering coefficients between oil spilled sea surface and clean sea surface at different wind speeds.

As can be seen in **Figure 6** and **Figure 7** above, significant differences in MSS and scattering coefficients between the overlying oil and the clean sea surface are observed under different wind speed conditions. Specifically, the differences in MSS

and scattering coefficients between oil and seawater are small when the wind speed is less than or equal to 2 m/s. This phenomenon may be due to the limited value of sea surface wave amplitude caused by low wind speed, which is insufficient to show significant differences in the physical properties of oil and seawater. Therefore, the similarity of MSS and scattering coefficients between the oil spill area and the surrounding seawater in a low wind speed environment poses a certain degree of challenge for oil spill detection. When the wind speed exceeds 2 m/s, there are obvious differences in MSS and scattering coefficients between oil and seawater.

4.2. CYGNSS Empirical Evidence

The preceding study analyzed the feasibility of using GNSS-R technology to detect marine oil spills from a simulation perspective. To verify the accuracy and reliability of the simulation results and further demonstrate the effectiveness and potential of GNSS-R in real marine environments for oil spill detection, this section conducts an empirical analysis using CYGNSS satellite-borne DDM data related to the Symphony tanker oil spill incident that occurred in 2021.

The incident occurred in the southeastern offshore waters of Zhaolian Island, Qingdao, Shandong Province, China, with the central coordinates located at 35˚43'8"N, 120˚58'5"E. To capture the impact of the oil spill distribution on GNSS-R signal characteristics in this region, CYGNSS constellation data collected between 00:00 and 24:00 on April 30, 2021, were extracted, as shown in **Figure 8**. **Figure 8** displays the remote sensing background image of the affected area along with the spatial distribution of CYGNSS observations during the corresponding

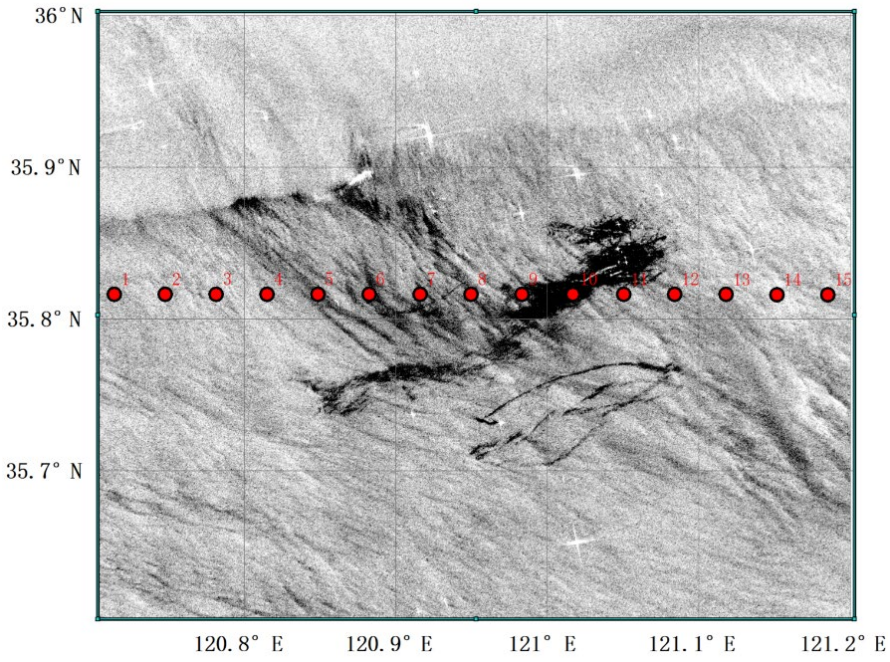

Figure 8. Symphony cargo ship oil spill experimental scenario (30 April 2021, CYGNSS data distribution).

time period. The red dots represent the projected positions of GNSS-R specular reflection points. These reflection points are concentrated around the 35.8˚N latitude line, spanning longitudinally from approximately 120.75˚E to 121.25˚E, with a coverage width of about 0.5˚, effectively encompassing the main area of oil contamination. This spatial-temporal alignment provides a critical data foundation for subsequent DDM analysis and oil spill identification.

This section also utilizes ERA5 sea surface wind data from the European Centre for Medium-Range Weather Forecasts (ECMWF), which correspond spatially and temporally to the CYGNSS satellite observations. ERA5 data offer high temporal and spatial resolution, reaching 1 hour and 0.125˚ × 0.125˚, respectively. To further improve the accuracy of wind field characterization in the study area, bilinear interpolation was applied to enhance the spatial resolution. The resulting sea surface wind distribution in and around the oil spill region is shown in **Figure 9**.

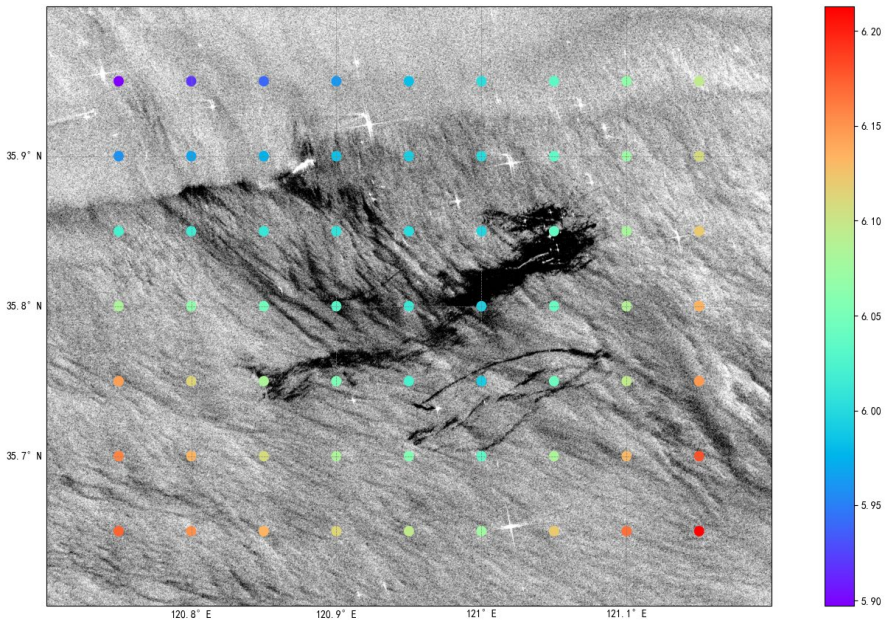

Figure 9. Distribution of sea surface wind speed in the synchronous space region of CYGNSS satellite data.

During the event, wind speeds in the oil spill area remained between 5.9 m/s and 6.2 m/s, with no wave breaking observed, indicating relatively calm sea conditions. Under such environmental conditions, the application of GNSS-R technology for oil spill information extraction and feature analysis is highly feasible. As shown in **Figure 10(a)**, the Delay-Doppler Map (DDM) corresponds to the clean sea surface obtained by CYGNSS-R, while **Figure 10(b)** presents the DDM image associated with the oil-contaminated area.

As shown in **Figure 10(a)**, the Delay-Doppler Map (DDM) of a clean sea surface acquired by CYGNSS exhibits a structure similar to that of the simulated clean sea surface DDM. Both display typical GNSS-R signal characteristics: the power reaches its maximum at the specular reflection point and forms a distinct

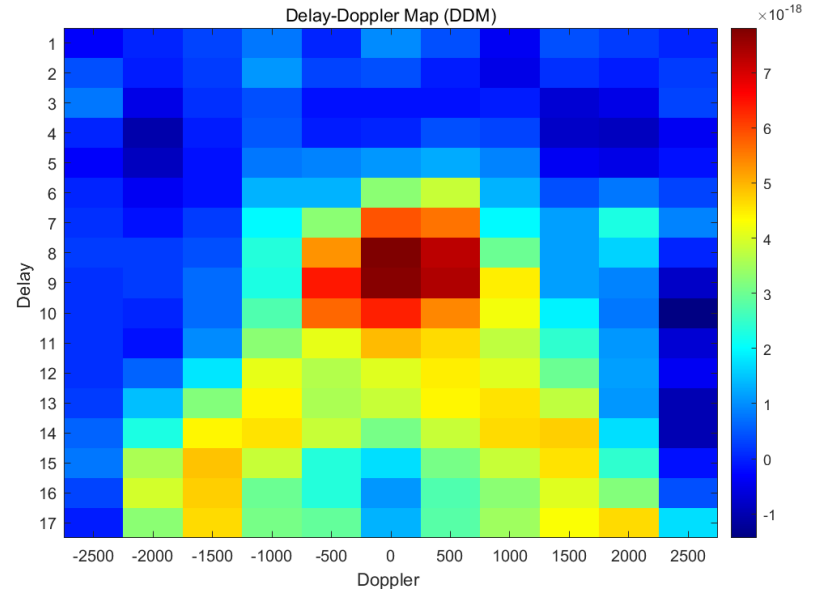

(a)

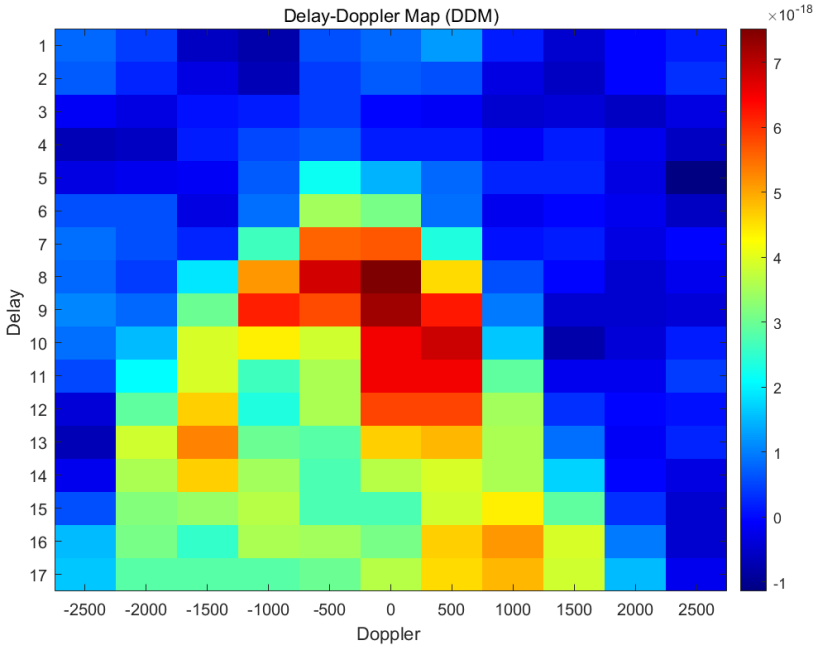

(b)

Figure 10. DDM images of clean sea surface and oil spill area from CYGNSS satellites. (a) Clean Sea Surface; (b) Oil Spill Area.

symmetric "horseshoe-shaped" distribution near the zero Doppler frequency line. However, **Figure 10(b)** illustrates the DDM corresponding to an actual oil spill area, where the power distribution near the specular reflection point shows abnormal variations, significantly differing from the "horseshoe-shaped" structure of the clean sea surface. Specifically, in certain delay-Doppler cells, the power is reduced, exhibiting localized asymmetry and weakened scattering intensity. This variation is primarily caused by the strong suppression of short-wave disturbances

by the surface oil film, which diminishes the presence of capillary and small-scale gravity waves, thereby significantly reducing local sea surface roughness and affecting the GNSS signal scattering response.

Overall, the measured DDM is influenced by multiple environmental factors, particularly wind speed and wind direction, which lead to spatial heterogeneity in sea surface roughness and cause asymmetry in the DDM image, with distinct scattering characteristics across different regions. These experimental results not only empirically validate the scientific basis and accuracy of the GNSS-R sea surface oil spill response model proposed in the earlier simulations, but also further emphasize the feasibility and effectiveness of using satellite-borne CYGNSS GNSS-R data for marine oil spill monitoring. With its high temporal resolution, wide spatial coverage, and strong sensitivity to sea surface conditions, CYGNSS is capable of providing stable and reliable observations under complex marine environments. Therefore, it offers critical technical support for rapid identification and dynamic monitoring of marine oil spill events, demonstrating the application potential and development prospects of GNSS-R technology in ocean remote sensing.

5. Conclusion

This study conducted a simulation-based investigation into marine oil spill monitoring using GNSS-R technology. By integrating the Z-V scattering model with the mean square slope (MSS) models for seawater and oil-covered surfaces, the 2021 Symphony tanker oil spill incident off the coast of Qingdao, China (April 27, 2021), was selected as the target scenario. Delay-Doppler Maps (DDMs) representing the reflective characteristics of the sea surface were simulated based on GNSS signal scattering. The simulation experiments, which accounted for surface asymmetry, demonstrated that GNSS-R DDMs can effectively identify oil-contaminated areas within a certain spatial range, confirming the feasibility of GNSS-R for oil spill detection. Further analysis revealed that sea surface wind speed significantly influences the simulation results. Specifically, when wind speed exceeds 2 m/s, both the scattering coefficient and DDM features over oil-covered areas exhibit pronounced anomalies, with their values decreasing as wind speed increases. This trend provides a theoretical foundation for interpreting GNSS-R signal behavior in oil-contaminated marine environments. By analyzing CYGNSS data corresponding to the Symphony tanker oil spill, changes in the peak power of DDMs over oil-covered areas were observed in the measured data. Near the specular reflection point, the DDM imagery clearly delineates the extent of the oil spill, further validating the characteristic GNSS-R response patterns derived from simulations. These findings confirm the effectiveness of using actual CYGNSS observations for marine oil spill detection and demonstrate the practical potential of GNSS-R technology in operational oil spill monitoring.

Funding

This work was supported by the Key Program of joint Fund of the National

Natural Science Foundation of China and Shandong Province under Grant U22A20586, the Natural Science Foundation of Shandong Province under Grant ZR2022MD015, the Fundamental Research Funds for the Central Universities under Grant 24CX02030A, the National Natural Science Foundation of China under Grant 41701513, 61371189, and 41772350, and the Key Research and Development Program of Shandong Province under Grant 2019GGX101033.

Acknowledgements

We extend our sincere gratitude to NASA for the provision of CYGNSS data.

Conflicts of Interest

The authors declare no conflicts of interest regarding the publication of this paper.

References

[1] Naz, S., Iqbal, M.F., Mahmood, I. and Allam, M. (2021) Marine Oil Spill Detection Using Synthetic Aperture Radar over Indian Ocean. *Marine Pollution Bulletin*, **162**, Article ID: 111921. https://doi.org/10.1016/j.marpolbul.2020.111921

[2] Zhu, Y., Qian, X., Liu, Z., Huang, P. and Yuan, M. (2015) Analysis and Assessment of the Qingdao Crude Oil Vapor Explosion Accident: Lessons Learnt. *Journal of Loss Prevention in the Process Industries*, **33**, 289-303. https://doi.org/10.1016/j.jlp.2015.01.004

[3] Brekke, C. and Solberg, A.H.S. (2005) Oil Spill Detection by Satellite Remote Sensing. *Remote Sensing of Environment*, **95**, 1-13. https://doi.org/10.1016/j.rse.2004.11.015

[4] Fan, J., Zhang, F., Zhao, D. and Wang, J. (2015) Oil Spill Monitoring Based on SAR Remote Sensing Imagery. *Aquatic Procedia*, **3**, 112-118. https://doi.org/10.1016/j.aqpro.2015.02.234

[5] Qi, Y., Zhang, B., Yang, D. and Li, B. (2019) Modeling and Simulation of GNSS Signal Reflected from the Ocean Surface. *Optik*, **180**, 1006-1017. https://doi.org/10.1016/j.ijleo.2018.11.140

[6] Zhang, Y., Liu, F., Gu, Q., Meng, W., Hong, Z. and Han, Y. (2013). Study of Accurate Ocean-Altimetry with GNSS-R. 2013 *IEEE International Geoscience and Remote Sensing Symposium*, Melbourne, 21-26 July 2013, 1410-1413. https://doi.org/10.1109/igarss.2013.6723048

[7] Martin-Neira, M. (1993) A Passive Reflectometry and Interferometry System (PARIS): Application to Ocean Altimetry. *ESA Journal*, **17**, 331-355.

[8] Rodriguez-Alvarez, N., Akos, D.M., Zavorotny, V.U., Smith, J.A., Camps, A. and Fairall, C.W. (2013) Airborne GNSS-R Wind Retrievals Using Delay-Doppler Maps. *IEEE Transactions on Geoscience and Remote Sensing*, **51**, 626-641. https://doi.org/10.1109/tgrs.2012.2196437

[9] Asgarimehr, M., Arnold, C., Weigel, T., Ruf, C. and Wickert, J. (2022) GNSS Reflectometry Global Ocean Wind Speed Using Deep Learning: Development and Assessment of CyGNSSnet. *Remote Sensing of Environment*, **269**, Article ID: 112801. https://doi.org/10.1016/j.rse.2021.112801

[10] Guo, W., Du, H., Guo, C., Southwell, B.J., Cheong, J.W. and Dempster, A.G. (2022) Information Fusion for GNSS-R Wind Speed Retrieval Using Statistically Modified Convolutional Neural Network. *Remote Sensing of Environment*, **272**, Article ID:

112934. https://doi.org/10.1016/j.rse.2022.112934

[11] Du, H., Li, W., Cardellach, E., Ribó, S., Rius, A. and Nan, Y. (2024) Deep Residual Fully Connected Network for GNSS-R Wind Speed Retrieval and Its Interpretation. *Remote Sensing of Environment*, **313**, Article ID: 114375. https://doi.org/10.1016/j.rse.2024.114375

[12] Fabra, F., Cardellach, E., Rius, A., Ribo, S., Oliveras, S., Nogues-Correig, O., *et al.* (2012) Phase Altimetry with Dual Polarization GNSS-R over Sea Ice. *IEEE Transactions on Geoscience and Remote Sensing*, **50**, 2112-2121. https://doi.org/10.1109/tgrs.2011.2172797

[13] Semmling, A.M., Rosel, A., Divine, D.V., Gerland, S., Stienne, G., Reboul, S., *et al.* (2019) Sea-Ice Concentration Derived from GNSS Reflection Measurements in Fram Strait. *IEEE Transactions on Geoscience and Remote Sensing*, **57**, 10350-10361. https://doi.org/10.1109/tgrs.2019.2933911

[14] Wang, F., Yang, D., Niu, M., Yang, L. and Zhang, B. (2022) Sea Ice Detection and Measurement Using Coastal GNSS Reflectometry: Analysis and Demonstration. *IEEE Journal of Selected Topics in Applied Earth Observations and Remote Sensing*, **15**, 136-149. https://doi.org/10.1109/jstars.2021.3133431

[15] Alonso Arroyo, A., Camps, A., Aguasca, A., Forte, G.F., Monerris, A., Rudiger, C., *et al.* (2014) Dual-Polarization GNSS-R Interference Pattern Technique for Soil Moisture Mapping. *IEEE Journal of Selected Topics in Applied Earth Observations and Remote Sensing*, **7**, 1533-1544. https://doi.org/10.1109/jstars.2014.2320792

[16] Guo, Z., Liu, B., Wan, W., Lu, F., Niu, X., Ji, R., *et al.* (2022) Soil Moisture Retrieval Using Bufeng-1 A/B Based on Land Surface Clustering Algorithm. *IEEE Journal of Selected Topics in Applied Earth Observations and Remote Sensing*, **15**, 4680-4689. https://doi.org/10.1109/jstars.2022.3179325

[17] Dai, S., Song, D. and Wang, B. (2025) CT-NET: A Cross-Modal Transformer Network for Satellite-Borne GNSS-R Soil Moisture Retrieval. *International Conference on Remote Sensing and Digital Earth* (*RSDE* 2024), Vol. 13514, 186-191. https://doi.org/10.1117/12.3059047

[18] Valencia, E., Camps, A., Marchan-Hernandez, J.F., Park, H., Bosch-Lluis, X., Rodriguez-Alvarez, N., *et al.* (2011) Ocean Surface's Scattering Coefficient Retrieval by Delay-Doppler Map Inversion. *IEEE Geoscience and Remote Sensing Letters*, **8**, 750-754. https://doi.org/10.1109/lgrs.2011.2107500

[19] Valencia, E., Camps, A., Rodriguez-Alvarez, N., Park, H. and Ramos-Perez, I. (2013) Using GNSS-R Imaging of the Ocean Surface for Oil Slick Detection. *IEEE Journal of Selected Topics in Applied Earth Observations and Remote Sensing*, **6**, 217-223. https://doi.org/10.1109/jstars.2012.2210392

[20] Li, C., Huang, W. and Gleason, S. (2015) Dual Antenna Space-Based GNSS-R Ocean Surface Mapping: Oil Slick and Tropical Cyclone Sensing. *IEEE Journal of Selected Topics in Applied Earth Observations and Remote Sensing*, **8**, 425-435. https://doi.org/10.1109/jstars.2014.2341581

[21] Li, C., Huang, W.M. and Wang, W. (2014) Simulation Based Tropical Cyclone Sensing Using Space-Based GNSS-R. 2014 *Oceans-St. John's*, St. John's, 14-19 September 2014, 1-4. https://doi.org/10.1109/oceans.2014.7003167

[22] Chen, S.S., Zhang, Y., Hong, Z.H., Han, Y.L. and Xie, X.F. (2017) Simulation Study on GNSS Reflected Signal Echo DDM for Marine Oil Spill Detection. *Global Positioning System*, **42**, 15-19.

[23] Zhang, Y., Chen, S., Hong, Z., Han, Y., Li, B., Yang, S., *et al.* (2017) Feasibility of Oil

Slick Detection Using Beidou-R Coastal Simulation. *Mathematical Problems in Engineering*, **2017**, Article ID: 9635854. https://doi.org/10.1155/2017/8098029

[24] Jia, Z.Y., Zhang, B., Wu, J., Yang, D.K. and Hong, X.B. (2018) Ground-Based GNSS-R Method for Marine Oil Spill Detection. *Journal of Beijing University of Aeronautics and Astronautics*, **44**, 383-390.

[25] Sun, Q.M., Zhang, B., Liu, J.H., Wang, L.F. and Jia, Z.Y. (2019) Oil Spill Area Detection on Sea Surface Using Ground-Based GNSS-R Platform. *Journal of Navigation and Positioning*, **7**, 88-95.

[26] Zavorotny, V.U. and Voronovich, A.G. (2000) Scattering of GPS Signals from the Ocean with Wind Remote Sensing Application. *IEEE Transactions on Geoscience and Remote Sensing*, **38**, 951-964. https://doi.org/10.1109/36.841977

[27] Cox, C. and Munk, W. (1954) Measurement of the Roughness of the Sea Surface from Photographs of the Sun's Glitter. *Journal of the Optical Society of America*, **44**, 838-850. https://doi.org/10.1364/josa.44.000838